

# A NEW METHOD TO DETECT THE ICME BOUNDARIES

C. DUMITRACHE AND N.A. POPESCU

*Astronomical Institute of Romanian Academy*

*Str. Cuitul de Argint 5,*

*040557 Bucharest, Romania*

*Email: crisd@aira.astro.ro; nedelia@aira.astro.ro*

*Abstract.* A new method to infer the boundaries of the interplanetary coronal mass ejections is proposed. The local minima of a proton temperature anisotropy are used as potential boundaries of the interplanetary event. The low-beta plasma values are then invoked to detect at least four boundaries, two for the beginning and two for the end of an interplanetary coronal mass ejection (ICME). Intermediate boundaries can be identified, as indicated by other plasma and magnetic field signatures, and mark substructures of an event. Using the algorithm we propose here, we have compiled a list with ICME events boundaries registered by *Ulysses* spacecraft during 2000-2002. Three magnetic clouds (observed on 23 January 2001, 10 June 2001 and 24 August 2001) are analysed with details. This method provides premises for an alternative way of automatic detection of the ICMEs boundaries.

*Key words:* Coronal Mass Ejections, Interplanetary . Solar Wind, Disturbances .

## 1. INTRODUCTION

Coronal mass ejections (CMEs) are the largest eruptive phenomena in the solar system responsible for drastic changes of the space weather conditions, directly affecting the life on Earth. The interplanetary CMEs counterparts expand from the Sun to heliosphere and produce disturbances of the interplanetary space. In-situ measurements of plasma and magnetic field display a wide range of signatures that guide us to identify the interplanetary coronal mass ejections (ICMEs) and their delimitations. Of these, widely invoked are: an intense magnetic field, the low-beta populations, density and velocity enhancements, increasing of ion charge states and abundance of various elements, as well as a decrease of the proton temperature. These properties are strengthened in the magnetic clouds (MCs), events that display a distinct morphology, with forward and reverse shocks, magnetic field smooth rotation, bi-directional electron streaming. MCs represent the interplanetary manifestation of a flux rope expelled from the Sun, and were first defined by Klein and Burlaga (1982) as regions with a radial dimension of approximately 0.25 AU at 1 AU, inside which the magnetic field strength is high.

There are ICMEs displaying all the features, while others have only a few. Along the years, different criteria have been used to identify the ICMEs or MCs Ri-

ley and Richardson (2013) statistically found that plasma beta, CME width, and the ratio  $O^{7+}/O^{6+}$  are significant variables that indicate the presence of an MC and the registration of an MC strongly depends on the spacecraft trajectory. In contrast to MC, the non-MC ICMEs could have weaker magnetic fields, higher proton temperatures, higher plasma beta, when comparing to the MCs, as Burlaga *et al.* (2001) reported. These ICMEs can be the result of the interaction of two or more MCs at lower heliocentric distances, and were called *complex ejecta* ICMEs (non-MCs). In the list built by Du, Zuo and Zhang (2010), with 181 ICMEs observed by *Ulysses* spacecraft, only 43% were identified as MCs. Richardson and Cane (2011) showed that MCs are more numerous at the solar minimum. Riley and Richardson (2013) described how the spacecraft trajectory influences the registration of an event and how observational data reveal or not the presence of an MC. They concluded that the interaction of two or more magnetic clouds gives as result a non-MC, *i.e.* a non-homogenous interplanetary structure. Using the Gaussian mixture model analysis, they identified three types of events from the ICMEs' speed vs. plasma beta correlation: (i) a statistical populations with low plasma beta and low velocities, (ii) another with high velocities and plasma beta, and (iii) a statistical population with low velocities but high plasma beta. In addition, we point-out as an useful tool to detect the presence of an MC and its boundaries, the minimum variance analysis (Klein and Burlaga, 1982; Bothmer and Schwenn, 1998; Dumitrache, Popescu, and Oncica, 2011), that proves a coherent rotation of the MCs around one axis, at the spacecraft encounter (Burlaga, 1988).

Many times, the ICMEs or MCs are merged, even if they left the Sun as distinct events. In this case, very often it is a challenge to detect the real boundaries of each one or how much two events are mixed, or to understand the mixed and non-mixed parts of a complex phenomenon. The solar source identification and analysis are useful in this case. But, Richardson and Cane (2010) have shown that it is possible to not really find the solar source for 46% of Earth directed ICMEs.

Beyond one astronomical unit (AU), the ICME identification become more difficult because of some ICME signatures are blurred through the interaction with the ambient solar wind. The *Ulysses* spacecraft's registrations for these long distances, as well as those obtained during its transient over the solar poles, are very important to help us understand how the high latitude CMEs travel through space, far from the ecliptic and beyond 1 AU, and have an insight to the 3D heliosphere.

The presence of an ICME in the interplanetary space is also accompanied by the charge states enhancement. The high values of the charge state of elements such as  $O$ ,  $C$ , and  $Fe$ , indicate the solar coronal origin of the ejected plasma. Lepri *et al.* (2001) considered the enhancement of  $Fe$  as the most reliable signature of an ICME. The values of  $Fe^{6+}$  to  $Fe^{16+}$  exceeding 11 represent an indicative for an ICME Lepri and Zurbuchen (2004). Another threshold that must be fulfilled by the

charge states is  $O^{7+}/O^{6+} > 0.8$  (Neugebauer and Goldstein, 1997), especially in MC (Henke *et al.*, 1998). The ICME threshold for the  $Fe/O$  rate is 0.25 (Zurbuchen and Richardson, 2006) and for  $C^{6+}/C^{5+}$  rate is 3. The elemental composition reflects the coronal source of the CME prior to the ejection into space: the most CMEs observed in the ecliptic plane reflect the photospheric composition (Reinard *et al.*, 2001). It seems that the enhancement of the charge states does not manifest in the sheath of MC - this aspect could help in better detecting the boundaries of an event. Henke *et al.* (1998) analyzed more ICMEs registered by *Ulysses* spacecraft and found that the MC structures have an increased  $O^{7+}/O^{6+}$  ratio compared to the non-MC ICMEs.

Russell and Shinde (2003) performed the ICMEs identification from the solar wind ion measurements. Signatures of an expanding magnetic structure were correlated with a decline in the solar wind speed, accompanied by simultaneous cool ions. These two indicators have long been associated with the occurrence of ICMEs (*e.g.* Gosling (1997) and references therein). Large deviations from thermal (Maxwellian) equilibrium are also expected due to the weakly collisional nature and adiabatic expansion of the solar wind away from the Sun. The most detailed results on observations of energetic distributions of plasma particles have indeed shown a suprathermal halo population always present in the solar wind, field-aligned beams (or even counterstreaming beams) in high-speed winds, and the temperature anisotropy more pronounced for the halo than for the core populations (Marsch *et al.*, 1982; Kasper *et al.*, 2002; Hellinger *et al.*, 2006; Matteini *et al.*, 2007). But the temperature anisotropy is in general lower than predictions from adiabatic expansion, and the most plausible constraints have been found to be the self-generated wave instabilities (Gary *et al.*, 2001; Kasper *et al.*, 2002; Hellinger *et al.*, 2006), such as the firehose for  $T_{\parallel} > T_{\perp}$  and the mirror or ion - cyclotron instabilities for  $T_{\parallel} < T_{\perp}$  (where  $\parallel$  and  $\perp$  denote directions parallel and, respectively, perpendicular to the local magnetic field). The upper and lower bounds of the temperature anisotropy  $A = T_{\perp}/T_{\parallel}$  fit reasonably well to the instability thresholds predicted by the linear theory. Marsch, Yao, and Tu (2009) have shown the existence of suprathermal protons and field-aligned beams in an ICME detected by Helios 2 on 3 April 1979. An isotropization of these suprathermal components becomes also apparent in the turbulent sheath between an ICME and the preceding shock (Skoug *et al.*, 2000; Reisenfeld *et al.*, 2003; Lazar *et al.*, 2014). Marsch *et al.* (1982) investigated the heliospheric radial gradient of the protons temperature anisotropy components, in the ecliptic plane, between 0.3 and 1 AU, for various solar wind velocities. They found the flattest radial profile for  $T_{\parallel}$  in the high speed wind and strong cooling in slow streams, while  $T_{\perp}$  exhibited a sharp radial decline, with no dependence on the solar wind speed. Although the plasma temperature decreases during an ICME event, the enhanced magnetic field strength in MCs is expected to increase the temperature anisotropy in perpendicular direction by compression. Estimates of the temperature anisotropy have been used

to explain turbulence responsible for heating in the ICMEs (Liu *et al.*, 2006a), the plasma depletion layers ahead of ICMEs (Liu *et al.*, 2006b). Marsch, Yao, and Tu (2009) previously found Alfvénic fluctuations at 0.7 AU, but these ones seem to not easy survive at longer distance in heliosphere. However, Liu *et al.* (2006b) detected turbulence supposed to drive from Alfvén waves at *Ulysses* orbit.

The problem of CMEs boundaries detection is crucial for space weather forecast, as well as for the phenomenon understanding. Not only one in-situ signature is sufficient to detect an event, but two or more criteria seems to be necessary in the event identification. Wei *et al.* (2003) analyzed more magnetic clouds at 1 AU and found distinct characteristics of plasma and magnetic fields inside the magnetic cloud bodies compared to the boundary layers. The front and reversal boundary layers, representing the interaction between the cloud and the surrounding interplanetary environment, are regions that display properties of magnetic reconnections, *i.e.* high proton density and temperature and plasma beta, but also abrupt azimuthal and latitudinal changes of the magnetic field. The outer boundary layer (between the sheath and the interplanetary environment) usually displays a drop in intensity of the magnetic field, while the inner boundary layer (which separates the interaction region from the cloud body) is associated with an initial rotation of the elevation angle and an enhancement of the magnetic field. Jamieson, Dalgarno, and Wei (2006) have performed a statistical analysis on 70 magnetic clouds registered by *Wind* spacecraft and found that the boundary layers are a non-pressure-balanced structure. Wang, Du and Richardson (2005) performed a multispacecraft analyse of the radial evolution of the ICME registered between 0.3 and 5.4 AU using the temperature decrease as a primary criterion for the events identification. They found that the temperature is a quantity that decreases slowly with the distance from the Sun, compared with other physical quantities. Du, Zuo and Zhang (2010) extended the list of events detected by Wang, Du and Richardson (2005), using the same criterion of identification and observations provided by *Ulysses*. Ebert *et al.* (2009) characterized the latitudinal and radial variations of the solar wind. They found no significative variations in latitude, but very important ones in the radial direction. They have extended the ICME list compiled by Gosling, Reisenfeld and Forsyth ([http://swoops.lanl.gov/cme\\_list.html](http://swoops.lanl.gov/cme_list.html)), using the pitch angle distribution measurements from *Ulysses* spacecraft and the magnetic field components to identify the ICMEs presence. Moreover, they used a combined set of signatures as lower than expected proton temperature, low plasma beta and high alpha particles density rated to the proton particles density. They accounted that an event is ICME if at least two criteria are fulfilled.

As Gosling (1997) stated, the ICMEs identification "is still something of an art", and this because of the multiple signatures to be tacked into account, but not all of them are always present for each event. For this reason we paid attention to another tool that can help us understanding different ICME events, in order to detect the

most appropriate boundaries and also to discriminate between pure or merged events. The aim of this paper is to detect more accurate the ICMEs boundaries and to understand the plasma process that are revealed by the interpretations of various plasma parameters. After analysing more events and compared the plasma characteristics, we have remarked that the temperature anisotropy variations delimitate the events' boundaries, *i.e.* a local minimum marks a boundary. An MC event is delimited by the interplanetary ambient forward and reverse shocks – these boundaries display a minimum value of the temperature anisotropy at the beginning and the end of the event. Liu *et al.* (2006a) found that  $T_{\perp}/T_{\parallel} \sim 1.2 - 1.3$  in the sheaths and lower in the solar wind. Inside an ICME, the temperature anisotropy increases considerable, but we can find more local minima that seem to delineate different structures of the event.

We analysed three specific MC events observed by *Ulysses* in 2001, on 10 June, 24 August and 23 January, in the light of a new boundary detection technique using the proton temperature anisotropy. We have investigated the morphology of these MC events for which we implement a new method to detect the event boundaries using the proton temperature anisotropy. After that, we have performed a statistic analysis of the data registered by *Ulysses* during three years, 2000, 2001 and 2002, when the spacecraft flew from negative to positive latitudes, also over the solar poles and from 1.34 AU to 4.47 AU distance from the Sun. The analysed period contains the years with maximum of CMEs production, after the sunspots maximum and during the solar general magnetic field polarity reversal.

Consequently, the article introduces the data and the method in section 2, while in section 4 we identify the ICME and MC events as result from the algorithm application for the period 2000-2002. Three specific case studies are described in section 3, where substructures of the MCs are detected and the established boundaries are verified with the minimum variance analyzes (MVA) tool.

## 2. DATA AND METHOD

The *Ulysses* spacecraft, launched in 1990, was the first mission that explored the Heliosphere from the solar equator to the poles. Gosling *et al.* (1994) first described the high-latitude ICMEs as a distinct events class. They showed that a forward-reverse shock pair is associated with each event and this is due to the over-expansion of the CME caused by its internal pressure. *Ulysses* provided plasma and magnetic field data until June 2009. In the present study we used data from three instruments onboard of *Ulysses*: VHM (magnetometer), SWOOPS (Solar Wind Plasma Experiment) and SWICS (Solar Wind Ion Composition Instrument).

For interplanetary events identification we have used the magnetic field data,

provided by VHM instrument and given in RTN coordinates, where R is the radial direction oriented from the Sun to the satellite, T is the cross product of the solar rotation axis and R, while N is the cross product of R and T. The magnetic field magnitude  $B$  and the  $(Br, Bt, Bn)$  components used in this paper had the time resolution of 1-hour. For the minimum variance analysis we used 1-minute time resolution data. The solar wind plasma parameters, *i.e.* the speed ( $v$ ), proton density ( $Np$ ), proton temperature ( $Tp$ ), were obtained by SWOOPS instrument, with hourly averaged data resolution. Information on the charge states plasma composition come from SWICS with 3-hour averaged data resolution.

The SWOOPS experiment was designed with two electrostatic analyzers for the solar wind investigation, one for positive ions and another for the electrons. The ions analyzer does not make an explicit ion species determination: the *separation* of protons from  $\alpha$  particles is made by the fact that both species have convection speeds. During the periods of spacecraft nutation, the amounts of the individual velocity components and temperatures are invalid and only the bulk speed and density are reliable. Taking into account that the spacecraft nutation ceased on the day 351 (DOY) of the year 1990, we are not concerned about these data alterations since our study focus on the years 2000, 2001 and 2002. The proton temperature has been estimated, by SWOOPS team, in two ways, providing two components,  $T_{\text{small}}$  and  $T_{\text{large}}$ , with direct indications of deviations from isotropy.  $T_{\text{large}}$  is the total numerical integral of the distribution in 3D velocity space over all energy channels and angle bins that are statistically above the noise. The quantity  $T_{\text{small}}$  is essentially the radial component of the temperature as it is estimated by summing over the angle of observations, and then integrating the resulting 1D moments over all energy channels.

Both quantities,  $T_{\text{small}}$  and  $T_{\text{large}}$ , enable us to compute the proton temperature,  $Tp$ , as a classical weighted geometric mean (Cranmer *et al.*, 2009):

$$Tp \equiv (T_{\text{large}} \cdot T_{\text{small}})^{1/2}. \quad (1)$$

One important signature for the ICME is also the temperature fall. During an ICME event, the proton temperature,  $Tp$ , rated to the expected temperature,  $T_{\text{exp}}$ , should be less than 0.5. This ratio depends on the solar wind speed, and it was computed for distances exceeding 1 AU (Wang, Du and Richardson, 2005) and speed, in  $10^3$  K units:

$$T_{\text{exp}} = \begin{cases} \frac{(0.031v-5.1)^2}{r^{0.7}}, & v < 500 \\ \frac{(0.51v-142)}{r^{0.7}}, & v \geq 500 \end{cases} \quad (2)$$

Another important rate of two temperatures is that of two quantities computed in the frame parallel and perpendicular to magnetic field direction, *i.e.*  $T_{\parallel}$  and  $T_{\perp}$ , known in the literatures as the temperature anisotropy,  $A \equiv \frac{T_{\perp}}{T_{\parallel}}$ . There are many works focussing on the protons temperature anisotropy, but we remind here the ar-

ticles of Kasper *et al.* (2006); Hellinger *et al.* (2006); Matteini *et al.* (2007) and especially the work of Podesta and Gary (2011) who used data from *Ulysses* spacecraft. Li *et al.* (1998) assumed the radial direction as the parallel direction and we adopt here this one, for the proton temperature anisotropy, and consider an anisotropy relative to the radial direction, *i.e.*  $Ar \equiv \frac{T_{\perp}}{T_{\parallel}}$ , with

$$T_{\parallel} \equiv T_{\text{small}}. \quad (3)$$

With the assumption that the space is an isotropic one, the perpendicular direction is computed from the formula:

$$T_{\perp} \equiv \frac{1}{2} (3T_p - T_{\parallel}). \quad (4)$$

Our aim is not to analyze the solar wind instabilities, but to have an insight on the ICMEs boundaries and substructures using the temperature anisotropy variations relative to the radial direction, since we have remarked the fall of  $Ar$  at the ICME boundaries. We propose here an algorithm to detect the ICMEs, where the various known signatures are applied in an hierarchical manner. For the computations of TAM we have found them if simultaneously  $Ar(i) < Ar(i-1)$  and  $Ar(i) < Ar(i+1)$ , where  $i$  denotes each registration inside a time period. To detect the possible boundaries, we have applied some threshold ( $pg$ ), retaining that TAM with  $Ar < pg$ . Usually, we have considered  $pg = 2.5$ , but  $pg$  could slightly differ from an event to another. The algorithm we have applied in our analysis implies more steps.

- Computation of the temperature anisotropy local minima (TAM), taking into account a certain threshold ( $pg$ ). These are the potential boundaries of the event.
- Plasma beta computation.
- Detection for each event(at least) four boundaries, such as:
  - First boundary ( $t1$ , expressed in DOY) is at the last TAM where  $\beta > 0.2$  before a region with  $\beta < 0.2$
  - Second boundary ( $t2$ , expressed in DOY) is at the first TAM with  $\beta < 0.2$ , following  $t1$
  - Third boundary ( $t3$ , expressed in DOY) is at the last TAM with  $\beta < 0.2$
  - Fourth boundary ( $t4$ , expressed in DOY) is at the following TAM with  $\beta > 0.2$ , following  $t3$
- Analyse of the total pressure variations for the event

After the raw estimation of the boundaries, other elements are taken into account for an event analysis, like the signatures of the proton temperature rated to the

expected temperature threshold inside the established boundaries, the charge states anomalies, as well as the enhanced total pressure during an event. The magnetic field components smooth rotation is an indicative for MC presence. There are also signatures for a complex morphology of an event that could indicate the existence of some substructures, as in the particular cases we have investigated here. The total protons pressure is expressed as the sum of the kinetic and magnetic pressures:

$$Pt = Np * k_B * T + B^2 / (8 * \pi). \quad (5)$$

where  $Np$  represents the proton number density and  $k_B$  is the Boltzman constant. Jamieson, Dalgarno, and Wei (2006) considered the MC boundaries as non-pressured-balanced structure. The total pressure will help us detect an event and its expansion in time (see the case studies).

### 3. CASE STUDIES

In this section we analyze in detail three MC events we found more spectacular, two of them have been summary analysed in previous papers by Popescu (2009) and Dumitrache and Popescu (2010). The first event (10 June 2001) can be found in the list of Du, Zuo and Zhang (2010), the second event (24 August 2001) is in the list of Ebert *et al.* (2009), while the last analysed event (23 January 2001) is found in both lists.

#### 3.1. THE 10 JUNE 2001 EVENT

The ICME event registered on 10 June 2001 (DOY=161) by *Ulysses* was produced by a series of explosive events occurred in the neighborhood of the active regions NOAA 09475 and 09486. Using hourly VHM data, 3-hours interval data from SWICS and hourly data from SWOOPS, onboard of *Ulysses* spacecraft, Dumitrache and Popescu (2010) studied this event for a duration of 38.4 hours, starting on day of the year DOY=161.2 and ending on DOY=162.8. At that date, the spacecraft was located at a distance of 1.35 AU from the Sun and at  $(19.6^\circ, 264.6^\circ)$  heliographic latitude and longitude (Du, Zuo and Zhang, 2010).

We have computed the event boundaries following the algorithm described in the previous sections, starting with the detection of the local minima of the temperature anisotropy. These local minima could be indicative of the isotropization of the field-aligned streams (or counterstreams), frequently observed in the boundary regions after the forward and reverse shocks (Skoug *et al.*, 2000; Steed *et al.*, 2011; Lazar *et al.*, 2014). Figure 1 displays the variation of the anisotropy  $Ar$ , together with the plot of the proton temperature rated to the expected one in the first panel. The vertical lines in the figure delineate these boundaries, while the horizontal lines indicate the thresholds for the computed quantities. The threshold imposed to  $T/T_{exp}$



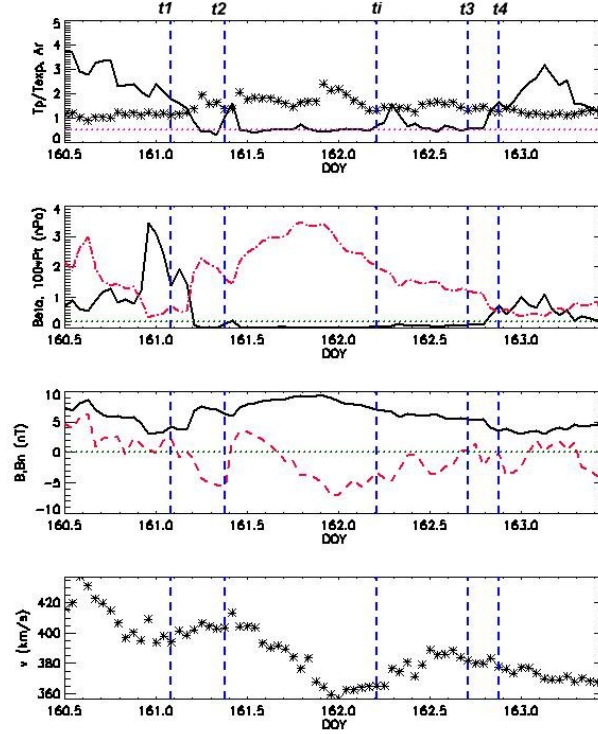


Fig. 1 – The event on 10 June 2001 – the vertical lines mark the boundaries, while the horizontal lines design the applied thresholds. 1st panel: The rate of proton temperature to the expected temperature,  $T/T_{exp}$  (solid line), and the temperature anisotropy  $Ar = T_{perp}/T_{parallel}$  (asterisks). 2nd panel: Variation of the protons beta (solid line) and total pressure (dot-dashed line). 3rd panel: Variation of the magnetic field total intensity  $B$  and of the normal component,  $B_n$ , in RTN coordinates ( $B$  – solid line,  $B_n$  – dashed line). 4th panel: Bulk velocity variations.

for the ICME condition fulfillment is (0.5). The TAM were computed as described in section 2 – we have retained as boundaries that TAM bordering the change of sign of the line  $\beta - 0.2$  (see 2). Figure 1 also displays the proton beta and the total pressure variations (second panel), together with 0.2 beta threshold. The total magnetic field magnitude and its normal component (in RTN coordinates) are displayed in the third panel, while the bulk velocity variations are plotted in the last panel. The obtained boundaries for the event are  $t1 = 161.083$ ,  $t2 = 161.375$ ,  $t3 = 162.708$ ,  $t4 = 162.875$ , expressed in days of the year (DOY).

As we noted in introduction, more signatures are necessary to identify an ICME and not all known signatures are fulfilled simultaneously to all events. Each author (Ebert *et al.*, 2009; Du, Zuo and Zhang, 2010; Wang, Du and Richardson, 2005) considered their own hierarchy in their compilations of the ICME list. In the present

article, after the TAM detection, we have retained those boundaries that delimited low plasma beta (see section 2). This condition is fulfilled between  $t_2$  and  $t_3$  boundaries, while  $t_1$  is the first TAM before  $t_2$  and  $t_4$  is the first TAM after  $t_3$ . The other signatures (fall of  $T/T_{exp}$  and the charge states anomaly) are considered as secondary criteria in our list. A very important variations are those of the total pressure; they indicate the event extension and represent an indicative to consider the extension of the boundaries to next TAMs, in some cases. We consider an internal boundary, at  $t_i = 162.21$ , where  $\beta = 0.04$ , at a computed TAM. The bulk velocity decreases from  $t_2$  to  $t_i$ , has a very slow increase at the end of the interval, and sudden variations between  $t_i$  and  $t_3$ . A decreasing period follows between  $t_3$  and  $t_4$ , inside the reverse shock zone.

This ICME displays many features of a magnetic cloud (Burlaga, 1995): smooth magnetic field rotates through a large angle, the strength of the magnetic field is higher than in the average solar wind, and the temperature is lower than that in the average solar wind. The enhanced field strength and smooth rotation of the vertical or azimuthal component are used to identify the MC event. The shape of these components indicates us if the event is an MC. The vertical lines delineate the boundaries of the forward (between  $t_1$  and  $t_2$ ) and reverse shocks and the core of the cloud (between  $t_3$  and  $t_4$ ), while the core is between  $t_2$  and  $t_3$ . We denoted with MC1 the first part of the core, between  $t_2$  and  $t_i$ , and with MC2 the second part of the cloud core, between  $t_i$  and  $t_3$ . The forward layer (sheath) is also marked by a drop of temperature, and a steep decline of the number density and the plasma beta. In order to identify the existence of the two or more cores of the cloud, we have applied the minimum variance analysis using 1-minute averaged data registered by VHM instrument.

According to Burlaga (1988), the MCs are also characterized by a smooth coherent rotation of the magnetic field parallel to a plane, when the spacecraft goes through the ICME considered as a flux rope. This rotation can occur in any direction on a time scale from few hours to days and can be revealed by the minimum variance analysis (MVA). The MVA was first time applied by Sonnerup and Cahill (1967). Klein and Burlaga (1982) and Bothmer and Schwenn (1998) described in detail the MVA method applied to MCs. The directional changes of the magnetic field can be investigated with the MVA applied to the field components in the spacecraft frame. Therefore, we pursue to detect these changes of all substructures of the magnetic cloud orientations in the Cartesian solar equatorial coordinates ( $X, Y, Z$ ), where  $B_x = -Br$ ,  $B_y = -Bt$ , and  $B_z = Bn$ , *i.e.*  $B_y$  pointing to the Est relative to the Sun (as described in Dumitrache, Popescu, and Oncica (2011)). This implies that RTN coordinates are rotated by  $180^\circ$  around the normal axis (Mulligan and Russel, 2001). After the MVA computations, we have obtained the magnetic field components of the clouds  $B_{xc}, B_{yc}, B_{zc}$  corresponding to the maximum variance, the intermediate and

minimum variance directions, respectively. The results are relevant if the rate of the eigenvalues corresponding to the intermediate and the minimum variance  $\lambda_2/\lambda_3 \geq 2$  and directional changes of the magnetic field vector exceed  $30^\circ$ . All these conditions are fulfilled in our computations for all three analysed events in this paper.

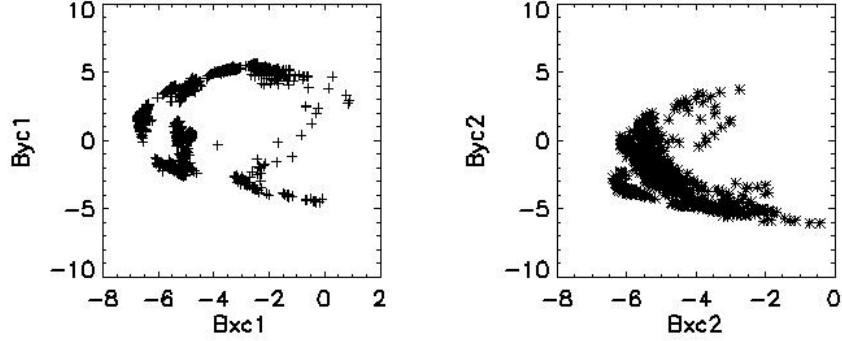


Fig. 2 – The 10 June 2001 event – MVA computations plot for the two cores of the MC.

Figure 2 shows our minimum variance analysis computation results, plotted in the intermediate-maximum variance plane (YOX) for both cores. The best results, indicating MC core subdivision, was obtained for two combinations: MC1 lasting from  $t_2$  to  $t_i$ , with 1199 registered points, and MC2 lasting from  $t_i$  to  $t_3$ , with 720 registered points. We have obtained the following rotation angles for the two cloud structures:

$$\begin{aligned} \phi_1 &= (171.82, 107.80, 107.80), \theta_1 = (22.97, -90.00, 90.00), \\ \phi_2 &= (166.01, 179.99, 90.81), \theta_2 = (1.93, -90.00, 90.00). \end{aligned}$$

We remark slightly different rotations of the cores MC1 and MC2, but remember the solar sources – there where flares coming from two different active regions.

The asymmetry of the charge states reveals also more cores for this event observed by *Ulysses*. Figure 3 displays the plots of charge states variations of  $C^{6+}/C^{5+}$ ,  $O^{7+}/O^{6+}$ , and  $Fe/O$  rates, and  $Q_{Fe}$  charge state, with their specific thresholds. We note the peak of the pressure in the first core, just like the  $O^{7+}/O^{6+}$  and  $Q_{Fe}$ . The first core of the event displays a high rate of  $O^{7+}/O^{6+} > 1$ , that is a typical signature for an MC. After that,  $O^{7+}/O^{6+} < 1$  for the second core. Low ratios of  $O^{7+}/O^{6+}$  and  $C^{6+}/C^{5+} < 3$  are indicative for fast streams. A high rate of the  $C^{6+}/C^{5+}$  is present in both cores, but with a fall at the end of the first core. The average  $Fe$  charge state,  $Q_{Fe}$ , is high only for the first core, while the rate  $Fe/O$  exceeds the threshold for ICME during all the event, but with a spectacular enhancement for the second core. The temperature values of the ions of  $O^{6+}$  and  $C^{6+}$  are low during the

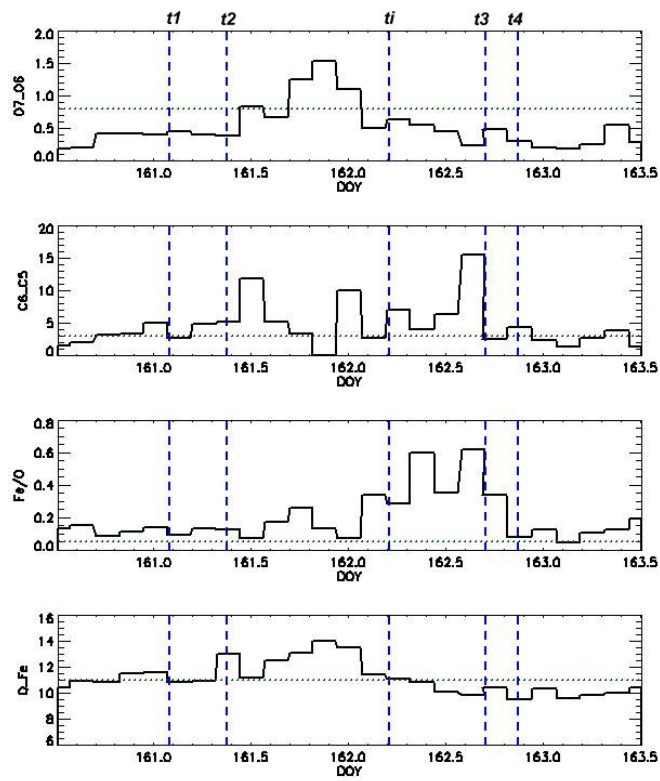


Fig. 3 – The 10 June 2001 event – charge states variation of  $O^{7+}/O^{6+}$ ,  $C^{6+}/C^{5+}$  rates,  $Fe/O$  rate and  $Q_{Fe}$  charge states. The vertical lines mark the boundaries, while the horizontal lines design the applied thresholds.

entire event.

The difference in the charge states measured between the components of the MC cores, as well as the variation of the bulk velocity, indicate us that actually are two different merged clouds or merged events that could belong to different solar sources. We remind the nature of the solar source of this event: more flares occurred in two active regions.

### 3.2. THE 24 AUGUST 2001 EVENT

Another MC event was observed by *Ulysses* (located at 1.68 AU and  $285.5^\circ$  longitude,  $67.3^\circ$  latitude) on 24 August 2001, *i.e.* DOY=236 Popescu (2009); Ebert *et al.* (2009). The tracking back to the Sun of this event, using a graphical method described in Dumitrache, Popescu, and Oncica (2011), gave us a raw estimation of the solar source as a CME starting from the Sun at DOY=230.25. The CDAW catalogue ([http://cdaw.gsfc.nasa.gov/CME\\_list](http://cdaw.gsfc.nasa.gov/CME_list)) indicates, as possible solar ICME counterparts, two CME in squall occurred at the polar angle  $PA \sim 337^\circ$ , but having too small velocities compared to the in-situ measured arrival speed ( $530 \text{ km s}^{-1}$ ). This event occurred on 15 August 2001 (DOY=227), at 10:30 UT, with  $v=311 \text{ km s}^{-1}$ . A linear propagation model of CME indicates the arrival of this event at *Ulysses* in the proper time, but it remains the problem with the speed, if we do not suppose that the ICME was accelerated by the ambient solar wind. Another candidate for the solar source is the halo CME occurred on 19 August 2001 (DOY=231), 6:06 UT, in or nearby the active region NOAA 09575, with the speed  $v=556 \text{ km s}^{-1}$ . The first candidate event belongs to a series of CMEs coming from a double sigmoid polar filament, while the second one is probable due to a flare.

Figure 4 displays the variations of plasma characteristics and magnetic field for this event. We have detected the four boundaries by computations of TAM, at  $t_1 = 235.833$ ,  $t_2 = 236.458$ ,  $t_3 = 237.917$ , and  $t_4 = 238.167$ . The bulk velocity of the solar wind displays a discontinuity, a shock, at  $t_i = 237.0$ , moment that indicates an intermediate (internal) boundary. Similar jump is observed at  $t_i$  for the  $Ar$  variation in time. It is also the moment of the peak (in absolute value) of the normal component of the magnetic field. We remark the temperature ratio  $T/T_{exp}$  decreasing under the corresponding threshold between  $t_2$  and  $t_3$ , and an increase over the threshold between  $t_3$  and  $t_4$ . The total pressure also peaks between  $t_2$  and  $t_i$ , following the  $Bn$  shape looked in mirror. The normal component of the magnetic field has two local extrema, in both region of the core event.

We have performed the MVA computation for first core, between  $t_2$  and  $t_i$  (781 points), and between  $t_i$  and  $t_3$  (1320 points). The result is displayed in figure 5, where we remark coherent smooth rotation only for the first core. Consequently, we have a MC only between  $t_2$  and  $t_i$ , while the second substructure is a simple ICME

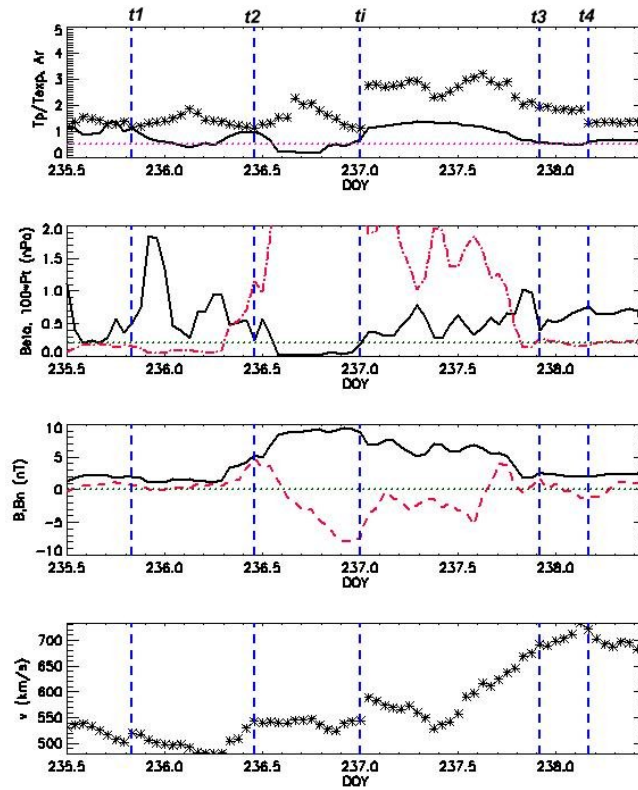


Fig. 4 – The event on 24 August 2001 – the vertical lines mark the boundaries, while the horizontal lines design the applied thresholds. 1st panel: The rate of proton temperature to the expected temperature,  $T/T_{exp}$  (solid line), and the temperature anisotropy  $Ar = T_{perp}/T_{parallel}$  (asterisks). 2nd panel: Variation of the protons beta (solid line) and total pressure (dot-dashed line). 3rd panel: Variation of the magnetic field total intensity  $B$  and of the normal component,  $B_n$ , in RTN coordinates ( $B$  – solid line,  $B_n$  – dashed line). 4th panel: Bulk velocity variations.

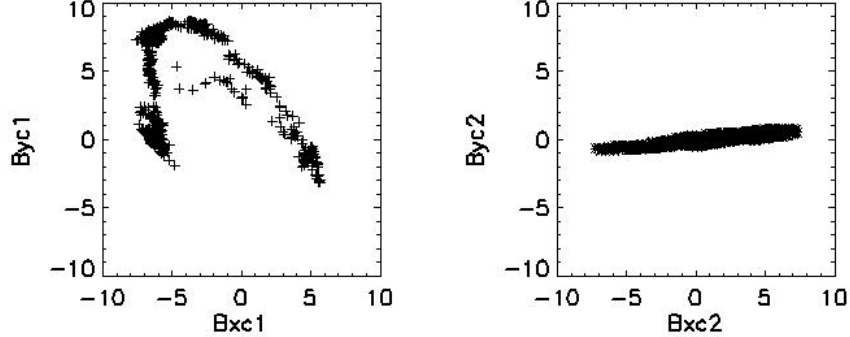


Fig. 5 – The 24 August 2001 event – MVA computations plot for the MC.

or other event that merged with the reverse shock of the MC.

For the MC we obtained the following rotation angles:

$$\phi = (143.29, 112.78, 180.00), \theta = (44.65, -89.93, 90.00).$$

During the second structure of the core, between  $t_i$  and  $t_3$ , the velocity decreases a period but spectacularly increases after that, continuing to increase also between  $t_3$  and  $t_4$ , with a peak of  $700 \text{ km s}^{-1}$  on the last border. The decreasing part of the velocity probably mark the reverse shock of the MC (near DOY=237.4 that does not coincide with a TAM).

The charge state distributions indicate weak characteristics for this event (figure 6). It seems that only the  $C^{6+}/C^{5+}$  and  $Fe/O$  overcome the corresponding threshold. A remarkable peak of the  $C^{6+}/C^{5+}$  is registered in the forward shock region and it is comparable with that inside the core of the MC.  $Q_{Fe}$  exceeds the corresponding threshold only in the forward shock. Gopalswamy *et al.* (2013) have found a significant difference between the boundaries derived from the solar wind plasma and magnetic signatures and that from the charge states signature. They considered that the charge states signatures start before the ICME boundary and such explain their enhancement in the sheaths for many events. They suggest a non-uniform repartition of the charge states during the entire ICME.

Figure 7 displays the velocity vs. protons beta plot. For  $\beta < 0.2$ , we remark the MC velocity ranging in the  $[520, 550] \text{ km s}^{-1}$  interval: this aspect could help us to expect that the solar source of this ICME is the flare from AR 09575. But a more speeded event follows this one and compose the second part of the 24 August 2001 ICME, interacting with the leading MC or with its reverse shock.

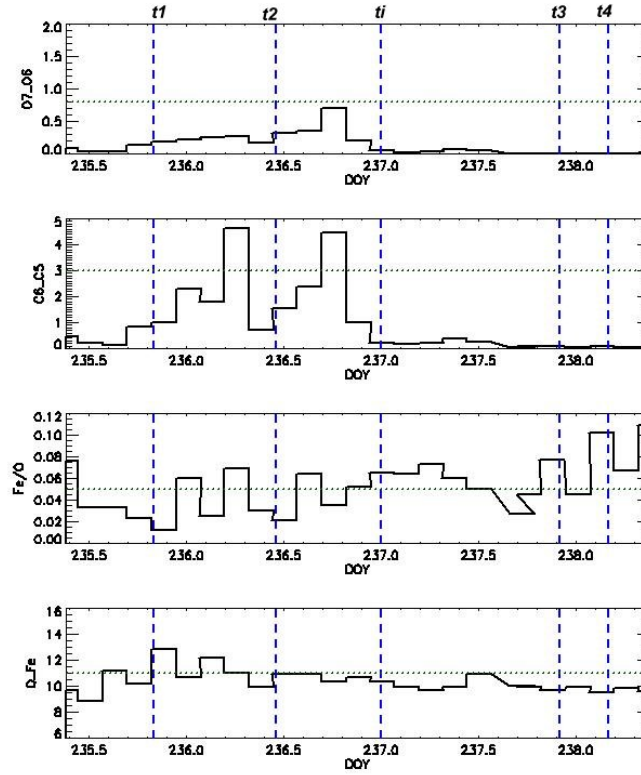


Fig. 6 – The 24 August 2001 event – charge states variation of  $O^{7+}/O^{6+}$ ,  $C^{6+}/C^{5+}$  rates,  $Fe/O$  rate and  $Q_{Fe}$  charge states. The vertical lines mark the boundaries, while the horizontal lines design the applied thresholds.

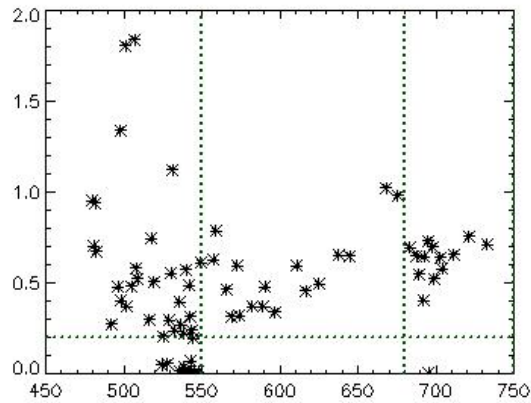


Fig. 7 – The 24 August 2001 event – the solar wind velocity vs. protons' beta.



### 3.3. THE 23 JANUARY 2001 EVENT

Two halo CMEs, registered by CDAW catalogue, came from two X-flares on 20 January 2001: first CME occurred at 19:31 UT, with a speed of  $839 \text{ km s}^{-1}$  and the second at 21:30 UT, with  $1507 \text{ km s}^{-1}$ . These flares occurred in the active region NOAA 09313. Considering a linear propagation, the corresponding interplanetary counterparts of those CMEs should hit the spacecraft, located at 1.88 AU,  $236.2^\circ$  longitude and  $-67.6^\circ$  latitude, on 23 January and 22 January respectively. A well-defined MC was observed by *Ulysses* starting with 23 January 2001 (Ebert *et al.*, 2009; Du, Zuo and Zhang, 2010).

Using the method proposed in this article, we have obtained the following boundaries:  $t1 = 23.75$ ,  $t2 = 23.875$ ,  $t3 = 24.792$ , and  $t4 = 25.042$ .

This event also has internal TAM as potential internal boundaries, at DOY 24.29 and 24.62, that correspond to the local peak of  $Tp/Temp$  rate and to the inflexion point of  $Bn$ , respectively. We have decided which one, or both, represent an internal boundary by the MVA, since the shape of the magnetic field components indicate us the presence of at least one MC. We found that  $ti = 24.29$  is an internal boundary that delineates two MCs (see later explanations).

Figure 8 displays the characteristics of this event: the temperature anisotropy and the proton temperature rated to the expected one, plasma beta variations and pressure, magnetic field and velocity variations. The total pressure peaks during the second MC core, while the tangential component of the magnetic field has an abrupt variation and peaks also during the second substructure. The velocity has a smooth decrease during both core structures (MC1 and MC2) and a sudden increase during the reverse shock (between  $t3$  and  $t4$ ).

The MVA reveals coherent rotations for two MC, as is display in figure 9.

The MVA computations were performed for 600 points (from  $t2$  to  $ti$ ) and for 720 points (from  $ti$  to  $t3$ ), giving the rotations angles:

$$\phi1 = (240.80, 129.52, 180.00), \theta1 = (21.44, -90.00, 90.00),$$

$$\phi2 = (208.14, 155.24, 155.24), \theta2 = (22.95, 90.00, 90.00).$$

Figure 10 plots the charge states of the event. We notice that the  $O^{7+}/O^{6+}$  rate does not attain the MC threshold, while  $C^{6+}/C^{5+}$  reaches once the threshold at the boundary between MC1 with MC2. The  $Fe$  hallmark attains the threshold during both MC's cores, but the rate  $Fe/O$  is really spectacular from the precursors zone and lasting after the end of the MC reverse shock, and has the peak during MC1.

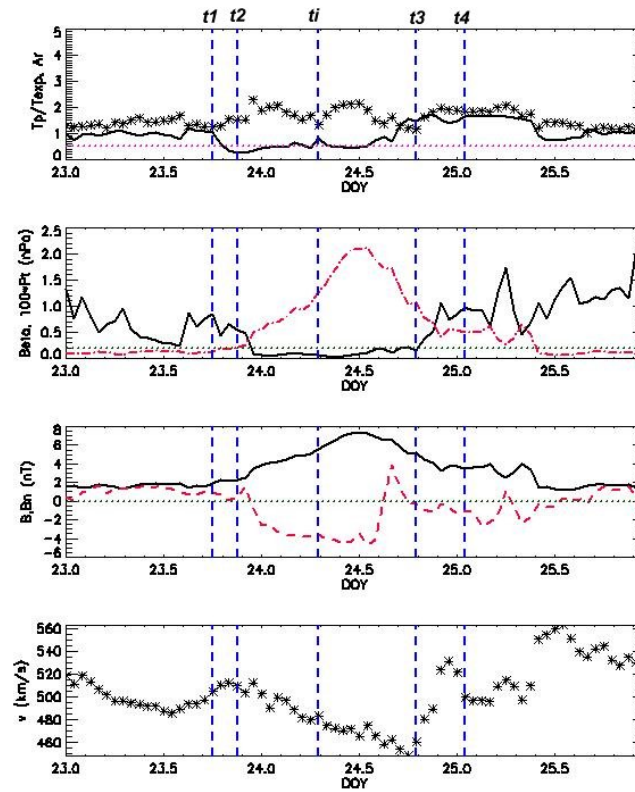


Fig. 8 – The event on 23 January 2001 – the vertical lines mark the boundaries, while the horizontal lines design the applied thresholds. 1st panel: The rate of proton temperature to the expected temperature,  $T/T_{exp}$  (solid line), and the temperature anisotropy  $Ar = T_{perp}/T_{parallel}$  (asterisks). 2nd panel: Variation of the protons beta (solid line) and total pressure (dot-dashed line). 3rd panel: Variation of the magnetic field total intensity  $B$  and of the normal component,  $B_n$ , in RTN coordinates ( $B$  – solid line,  $B_n$  – dashed line). 4th panel: Bulk velocity variations.

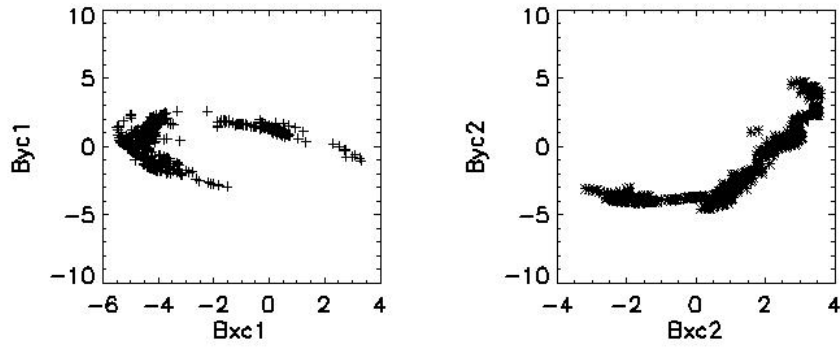


Fig. 9 – The 23 January event – MVA computations plot for the MC.

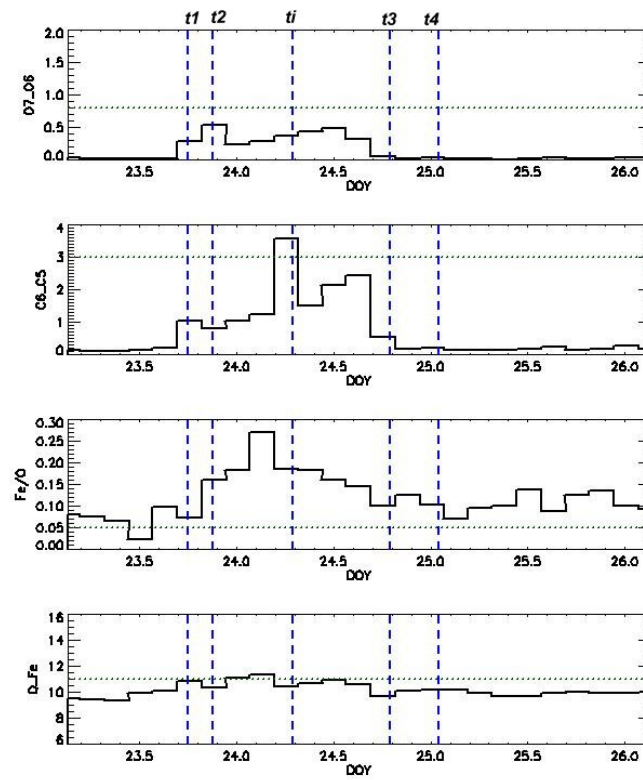


Fig. 10 – The 23 January 2001 event – charge states variation of  $O^{7+}/O^{6+}$ ,  $C^{6+}/C^{5+}$  rates,  $Fe/O$  rate and  $Q_{Fe}$  charge states. The vertical lines mark the boundaries, while the horizontal lines design the applied thresholds.

#### 4. ICMES LIST

We have applied the above described algorithm to compile a ICMEs list for a period of three important years of the solar cycle 23: 2000, 2001 and 2002. We have found 56 events, listed in the Table I. Among of these events, 2 are found in the list compiled by Du, Zuo and Zhang (2010), 8 are found in the Ebert *et al.* (2009) list, while 24 events are in both lists. We found 22 new events by following the criteria we introduced in this article. The majority of the events from Table I are non-MC (64%), while 36% are MCs.

The table contains the list of the events, as follows: each event line contains four boundaries  $t_1, t_2, t_3, t_4$  together with the corresponding velocity, proton beta and temperature anisotropy on these boundaries. The last column describes the type of the event, if a MC is present. For MC events,  $t_1$  and  $t_2$  define the boundaries of the forward shock and  $t_3$  and  $t_4$  define the boundaries of the reverse shock.

The  $t_1$  and  $t_4$  boundaries are roughly defined for  $\beta > 0.2$ , while  $t_2$  and  $t_3$  are established at the TAM with  $\beta < 0.2$ . There are few exceptions, namely when the aspect of the magnetic field and total pressure ( $Pt$ ) indicate a more extended event, where we have considered as boundaries the corresponding TAM.

The statistical computations give an average of the anisotropy at the boundaries of 1.37 (at the first boundary), 1.47 (at the second boundary), 1.41 (at the third boundary), and 1.36 (at the fourth boundary). The average of the plasma beta on the four boundaries are 0.63, 0.24, 0.18, and 0.52, respectively. There are some events that extend more than that defined in the rules for beta (at the beginning or the end of the event), this being indicated by the pressure of magnetic field variations.

We notice that we have detected at least four boundaries for all events, but at a detailed analysis, an event could display substructures and additional internal boundaries could be necessary to be added, but these are also TAM.

#### 5. CONCLUSIONS

The prediction of CMEs' arrival time is an important goal for heliospheric researches. This prediction is linked to the propagation mode of the CME into the interplanetary space, but also to the accuracy of the ICME boundaries detection. Usually, these boundaries could be established by the analysis of magnetic field shape, or adding information about the plasma  $\beta$ , temperature, density, speed and charge states variation. We proposed here a new method to detect the interplanetary event boundaries using the temperature anisotropy local minima and the variations of plasma beta as principal criterion to delimitate the ICMEs. The algorithm we have applied here allowed us to compute the boundaries following few steps: TAM computation using a certain threshold (that could vary from an event to another), selection of those two

TAM that border a region with  $\beta < 0.2$  and also those two TAMs containing the previous interval and where  $\beta$  exceeds 0.2. The analysis of the total pressure variation, temperature, charge states and magnetic field signatures could be an indicative to extend or limit the boundaries of an event. In the individual cases analysis we could find that intermediate boundaries are necessary (belonging also to the computed TAM), if merged events exist. This method allow us to better understand the morphology of an event. We have computed the boundaries for the ICMEs occurred during the maximum of solar CME production period, *i.e.* the years 2000, 2001 and 2002 and found events listed also by other authors, but also few new small ICMEs.

In the individual cases analysis we could found that intermediate boundaries are necessary (belonging also to the computed TAM), if merged events exist. This method allow us to also understand the morphology of an event. We have analysed the morphology of three known MCs: events registered on 10 June 2001, 24 August 2001 and 23 January 2001. We found that the MC registered by *Ulysses* on 10 June 2001 is actually a complex structure of two MC events, resulted from a series of flares occurred in the NOAA active regions 09475 and 09486. Similar story has also the event observed by *Ulysses* on 23 January 2001. The two merged MCs came from the two rapid halo CMEs occurred after flares raised in NOAA 09313, and probably traveled together. A different status has the event from 24 August 2001, where a single MC was detected.

The computed  $T_{\perp}$  and  $T_{\parallel}$  display jumps in certain regions, corresponding to the boundaries or in their vicinity and we suppose these regions actually mark distinct flow regimes. These distinct flow regimes delineate the different parts of an ICME or MC. This remark helped us to accurately establish the event boundaries and internal structure. The solar wind expands outward from the Sun, fulfilling the Parker spiral of the magnetic field lines. A significant ICME event contains plasma frozen in an enhanced magnetic field and, for speed exceeding that of the solar wind, it propagates almost radially. An interplanetary event has also a certain width, not at all negligible. The increased magnetic field and particle density number allow the increase of the total pressure during an ICME. In these circumstances, a certain isotropy of the solar wind temperature is broken around the ICME and a significant perpendicular anisotropy arises. This fact implies an increase of  $Ar > 1$ , greater than the normal anisotropy that appear in the ordinary solar wind. An ICME event is characterized by very low plasma beta, so by an important internal magnetic pressure. This explains why during the event the spacecraft registers temperatures with high anisotropy, exceeding 1 – 1.5 value. But an ICME or an MC could have a fragmentary structure due to different events interaction or even due to the magnetic tube ropes filamentary structure. That is why, more local minima could exist inside an event: when the spacecraft register a compact structure,  $Ar$  is large, when a boundary between component structures is registered,  $Ar$  decreases temporary since the anisotropy tends to

become stable. This process could explain the good enough correspondence between ICME boundaries and the local minima of the temperature anisotropy.

In conclusion, using the proton temperature anisotropy for ICMEs events registered by *Ulysses*, we were able to establish the event boundaries and developed an algorithm, boundaries that previously were settled up by the scientist expertise and experience to find them. Moreover, we have detected the case when merged events occurred. There are also additional information we could extract from the above analysis, such as the charge states asymmetry.

This method was set up here in the case of *Ulysses* spacecraft, but the principle of the algorithm described in this article could be used for other satellites too and offers the premise for an automatic detection method of the ICMEs boundaries.

*Acknowledgements.* The CME catalog is generated and maintained at the CDAW Data Center by NASA and The Catholic University of America in cooperation with the Naval Research Laboratory, and use data from SOHO. *Ulysses* and SOHO are projects of international cooperation between ESA and NASA. We acknowledge the National Space Science Data Center and the Principal Investigator, A. Balogh of Imperial College, London, UK, for the VHM data.

We thank Dr. Marian Lazar (Ruhr-Universitt Bochum) for useful discussions on this topic.

#### REFERENCES

- Bothmer, V., Schwenn, R. 1998, *Annales Geophysicae* **16**, 1
- Burlaga, L. F. 1988, *J. Geophys. Res.* **93**, 7217.
- Burlaga, L.F., Skoug, R.M., Smith, C.W., Webb, D.F., Zurbuchen, T.H., and Reinard, A. 2001, *J. Geophys. Res.* **106**, 20957
- Burlaga L. F.: 1995 *ISAA* **3**
- Cranmer, S.R., Matthaeus, W.H., Breech, B.A., and Kasper, J.C. 2009, *Astrophys. J.* **702**, 1604
- Du, D., Zuo, P.B., Zhang, X.X. 2010, *Solar Phys.* **262**, 171
- Dumitrache, C., Popescu, N.A.: 2010, in *IAGA Second Symp.Proc.*, Cairo Univ.Press., eds. L.Dame, A.Hady, 201
- Dumitrache, C., Popescu, N.A., and Oncica, A. 2011, *Solar Phys.* **272**, 137
- Ebert, R. W., McComas, D. J., Elliott, H. A., Forsyth, R. J., Gosling, J. T. 2009, *J. Geophys. Res.* **114**, 1109
- Gary, S. P., Skoug, R. M., Steinberg, J. T., Smith, C. W. 2001, *Geophys. Res. Lett.* **28**, 2759
- Gopalswamy, N., Mäkelä, P., Akiyama, S., Xie, H., Yashiro, S., Reinard, A. A. 2013, *Solar Phys.* **284**, 17
- Gosling, J.T., McComas, D.J., Phillips, J.L., Weiss, L.A., Pizzo, V.J., Goldstein, B.E., and Forsyth, R.J. 1994, *Geophys. Res. Lett.* **21**, 2271
- Gosling, J. T. 1997, in N. Crooker, J. A. Joselyn, and J. Feynman (eds.), *Coronal Mass Ejections*, AGU, Washington D. C., 9
- Hellinger, P., Travnicek, P., Kasper, J. C., and Lazarus, A. J. 2006, *Geophys. Res. Lett.* **33**, 9101
- Henke, T., Woch, J., Mall, U., Livi, S., Wilken, B., Schwenn, R., Gloeckler, G., von Steiger, R., Forsyth, R.J., Balogh, A. 1998, *Geophys. Res. Lett.* **25**, 3465
- Kasper, J. C., Lazarus, A. J., and Gary, S. P. 2002, *Geophys. Res. Lett.* **29**, 20-1

- Kasper, J.C., Lazarus, A.J., Steinberg, J.T., Ogilvie, K.W., and Szabo, A. 2006, *J.Geophys.Res. A* **111**, 3105
- Klein, L.W., Burlaga, L.F. 1982, *J. Geophys. Res.* **87**, 613
- Lazar, M., Pomoell, J., Poedts, S., Dumitrache, C., Popescu, N.A. 2014, *Solar Phys.*, submitted
- Lepri, S.T., Zurbuchen, T.H., Fisk, L.A., Richardson, I.G., Cane, H.V., and Gloeckler, G. 2001, *J. Geophys. Res.* **106**, 29231
- Lepri, S.T., Zurbuchen, T.H. 2004, *J. Geophys. Res.* **109**, A6, 2312
- Li, X., Habbal, S.R., Kohl, J., and Noci, G. 1998, *Astrophys. J.* **501**, L133
- Liu, Y., Richardson, J.D., Belcher, J.W., Kasper, J.C., and Skoug, R.M. 2006, *J.Geophys.Res. A* **111**, A01102
- Liu, Y., Richardson, J. D., Belcher, J. W., Kasper, J. C., Skoug, R. M. 2006, *J. Geophys. Res.* **111**, A09108
- Marsch, E., Muhlhauer, K.H., Schwenn, R., Rosenbauer, H., Pilipp, W., Neubauer, F. M. 1982, *J. Geophys. Res.* **87**, 52
- Marsch E., Yao S., Tu C.-Y. 2009, *Annales Geophysicae* **27**, 869
- Matteini, L., Landi, S., Hellinger, P., Pantellini, F., Maksimovic, M., Velli, M., Goldstein, B. E., Marsch, E. 2007, *Geophys. Res. Lett.* **34**, 20105
- Mulligan, T., Russel, C.T. 2001, *J. Geophys. Res.* **106**, 10581
- Neugebauer, M., Goldstein, R. 1997, *Geophys. Monogr. Ser.* **99**, 245
- Podesta J. J., Gary S. P., 2011, *Astrophys. J.* **734**, 15
- Popescu, N.A. 2009, *IAU Symposium* **257**, 295
- Reinard, A.A., Zurbuchen, T.H., Fisk, L.A., Lepri, S.T., Skoug, R.M., and Gloeckler, G. 2001, *AIPC* **598**, 139
- Reisenfeld, D.B., Gosling, J.T., Forsyth, R.J., Riley, P., St. Cyr, O.C. 2003, *Geophys. Res. Lett.* **19**, 8031
- Riley, P. and Richardson, I.G. 2013, *Solar Phys.* **284**, 217
- Richardson, I.G. and Cane, H.V. 2010, *Solar Phys.* **264**, 189
- Richardson, I.G. and Cane, H.V. 2011, *AGU Fall Meeting Abstracts*, 1979
- Russell, C.T., Shinde, A.A. 2003, *Solar Phys.* **216**, 285
- Skoug, R., Feldman, W.C., Gosling, J.T., McComas, D.J. 2000, *J. Geophys. Res.* **105**, 23069
- Sonnerup, B. U. O. and Cahill, Jr., L. J. 1967, *J. Geophys. Res.* **72**, 171
- Steed, K., Owen, C.J., D emoulin, P., Dasso, S. 2011, *J. Geophys. Res.* **116**, A01106
- Wang, C., Du, D., Richardson, J. D. 2005, *J. Geophys. Res.* **110**, 10107
- Wei F., Liu R., Fan Q., Feng X. 2003, *J.Geophys.Res. A* **108**, 1263
- Wei F., Feng X., Yang F., Zhong D., 2006, *J.Geophys.Res. A* **111**, 3102
- Zhao, L., Zurbuchen, T. H., Fisk, L. A. 2009, *Geophys. Res. Lett.* **36**, L14104
- Zurbuchen, T. H., Richardson, I. G. 2006, *Space Sci. Rev.* **123**, 31

## 6. APPENDIX

Table I. The ICMEs list

No	t1 (DOY)	v1 (km s <sup>-1</sup> )	$\beta$ 1	Ar1	t2 (DOY)	v2 (km s <sup>-1</sup> )	$\beta$ 2	Ar2	t3 (DOY)	v3 (km s <sup>-1</sup> )	$\beta$ 3	Ar3	t4 (DOY)	v4 (km s <sup>-1</sup> )	$\beta$ 4	Ar4	Type	
		2000																
1	17.83	421.2	0.89	1.32	18.04	417.6	0.24	1.43	18.58	397.7	0.28	1.49	18.67	388.3	0.52	1.53		
2	39.25	551.5	0.92	1.77	39.46	539.8	0.17	1.39	39.92	545.9	0.2	1.32	40	530.3	0.78	1.31		
3	40.67	539.3	0.26	1.89	40.88	542.6	0.34	1.67	41.88	511.6	0.09	1.4	42	519.1	0.24	1.36		
4	45.79	449.7	0.84	1.04	45.88	450	1	1.09	46.83	430.3	0.59	1.15	47.04	427	0.36	1.33		
5	78.83	398.1	0.8	1.19	78.92	384.7	0.14	1.17	79.54	368.3	0.11	1.3	79.67	364.8	0.27	1.36	MC	
6	91.04	381.2	0.6	1.1	91.21	386.8	0.09	1.27	92.25	401.8	0.16	1.43	92.38	401.1	1.09	1.15	MC	
7	101.88	412.6	0.14	1.3	102	418.3	0.09	1.4	103.04	446	0.18	1.34	103.13	457.4	0.27	1.31		
8	103.67	431.4	0.34	1.32	103.79	426.6	0.12	1.3	105.17	438.1	0.28	1.83	105.25	443.8	0.4	1.92		
9	121.17	514.6	0.71	1.36	121.46	486	0.04	1.74	122.71	431.3	0.09	1.82	122.79	428.5	0.07	1.63		
10	132.58	435.3	0.7	1.9	133.88	465	0.09	1.53	135.29	443	0.11	1.14	135.5	457.2	0.41	1.16		
11	147.63	385.3	0.81	1.45	147.79	376.4	0.21	1.74	148.63	345.8	0.03	1.87	148.71	366.7	0.08	1.76		
12	176.88	354.9	0.46	1.89	177.71	341.8	0.23	1.92	178	342.9	0.18	1.71	178.13	341.3	0.2	1.89		
13	223.42	481.8	0.48	1.42	224.29	449.3	0.07	1.76	225.25	427.9	0.18	1.98	225.5	434.4	0.25	1.36	MC	
14	256.88	407.1	0.97	1.51	257.17	411.9	0.04	1.73	257.88	401.6	0.94	1.08	258.13	403.7	0.78	1.19		
15	294.04	368.1	0.51	1.12	294.46	404.3	0.42	1.13	294.88	413.8	0.22	1.17	295.21	456.7	2.3	1.21	MC	
16	341.33	445.8	0.42	1.55	341.58	423.1	0.14	1.88	342.33	371.5	0.09	1.84	342.71	359.6	0.49	1.38	MC	



Table I—Continued

No	t1 (DOY)	v1 (km s <sup>-1</sup> )	$\beta_1$	Ar1	t2 (DOY)	v2 (km s <sup>-1</sup> )	$\beta_2$	Ar2	t3 (DOY)	v3 (km s <sup>-1</sup> )	$\beta_3$	Ar3	t4 (DOY)	v4 (km s <sup>-1</sup> )	$\beta_4$	Ar4	Type
2001																	
17	23.75	504.8	0.85	1.25	23.88	509.6	0.53	1.53	24.79	460.8	0.15	1.16	25.04	499.6	0.99	1.83	MC
18	32.54	469.8	0.64	1.32	32.79	447.6	0.15	1.33	33.25	430.4	0.09	1.48	33.5	427	0.92	1.18	
19	80.42	354.4	0.22	1.23	80.63	360.1	0.17	1.04	80.88	346.4	0.24	0.84	81.33	355.8	0.48	1.18	
20	90.67	366.8	1.25	1.25	90.83	363.3	0.31	1.3	91.42	346.6	0.17	1.36	91.75	372.4	0.38	1.05	
21	92	373.9	0.29	1.07	92.38	327.5	0.14	1.48	93.08	304.9	0.06	1.07	93.33	387.3	0.25	1.15	
22	100.67	409.3	1.24	1.19	101.21	610.8	0.05	1.84	102.79	496.6	0.15	1.02	102.88	492.5	0.16	1.13	MC
23	110	537.5	0.17	1.57	110.58	903.4	0.03	1.38	112.5	543.7	0.1	1.17	112.67	537.4	0.15	0.99	
24	119.54	392.8	0.53	1.13	119.79	408.4	0.17	1.19	120.58	406.4	0.06	1.6	120.88	392.7	0.41	1.13	MC
25	123.96	368.8	0.36	1.43	124.13	361.2	0.17	1.14	124.63	359.9	0.09	1.14	124.83	361.2	0.3	0.86	
26	129.79	367.1	0.21	1.42	129.96	365.9	0.06	1.77	130.75	623.8	0.14	1.29	130.83	602.9	0.3	1.5	
27	139.13	425.8	0.41	1.15	139.29	433.9	0.1	1.28	140.25	390.2	0.13	1.21	140.46	393.6	0.23	1.12	
28	156.25	462.4	0.21	1.28	156.46	515.2	0.09	1.27	156.75	526.2	0.14	1.49	156.92	505.3	0.24	1.22	
29	161.08	394.1	1.39	1.11	161.38	403.6	0.13	1.37	162.71	381.9	0.11	1.32	162.88	377.8	0.72	1.26	MC
30	185.63	300.1	0.3	1.24	185.75	298.3	0.19	1.26	186.46	295.3	0.12	1.35	186.83	308.6	0.48	1.36	
31	187.21	303.8	0.48	1.22	187.42	303	0.13	1.25	188.25	300.8	0.05	1.35	188.54	294.4	0.45	1.15	
32	204.25	407.6	0.86	0.99	204.54	414.6	0.02	1.87	206	365.7	0.08	1.36	206.08	357.7	0.26	1.17	
33	235.83	519.4	0.5	1.19	236.46	543.3	0.24	1.15	237.92	691.9	0.4	1.93	238	698.6	0.52	1.85	MC

Table I—Continued

No	t1 (DOY)	v1 (km s <sup>-1</sup> )	$\beta_1$	Ar1	t2 (DOY)	v2 (km s <sup>-1</sup> )	$\beta_2$	Ar2	t3 (DOY)	v3 (km s <sup>-1</sup> )	$\beta_3$	Ar3	t4 (DOY)	v4 (km s <sup>-1</sup> )	$\beta_4$	Ar4	Type
2002																	
34	2.71	562.1	0.31	1.03	2.83	564.2	0.15	1.24	3.54	571.8	0.12	1.08	3.63	554.1	0.46	1.42	
35	18.04	531.5	0.37	1.79	18.42	502	0.08	1.92	19.17	500.5	0.15	1.81	19.29	484.5	0.24	1.48	MC
36	31.63	414.7	0.23	1.37	31.83	420.8	0.04	1.44	32.17	404.7	0.21	1.18	32.33	416.7	0.25	1.07	
37	32.46	412	0.47	1.16	32.63	396.3	0.08	1.55	32.88	405.1	0.1	1.33	33.04	430.6	0.65	1.18	
38	42.63	540.1	0.72	1.31	43.04	547.1	0.09	1.74	43.88	523	0.29	1.27	44.46	533	3.04	1.74	MC
39	73.17	489.7	1.05	1.27	73.42	504	0.18	1.5	73.96	484.7	0.27	1.32	74.08	496.4	0.27	1.33	MC
40	84.17	502.8	0.97	1.17	84.25	489	2.23	1.2	85.04	496.8	0.36	1.2	85.25	529	0.16	1.36	MC
41	97.21	369.7	0.86	1.28	97.42	410.8	0.18	1.36	97.58	400	0.12	1.31	97.67	386.7	1.16	1.22	MC
42	125.04	390.7	0.3	1.41	125.17	396.5	0.15	1.58	129.42	322.1	0.17	1.9	129.67	436.3	1	1.5	MC
43	154.83	493.2	3.28	1.18	155	470.9	1.01	1.23	155.08	479.2	0.19	1.2	155.17	500.6	0.12	1.16	
44	156.54	726.5	1.13	1.66	156.67	722.2	0.11	1.7	157.08	707.2	0.26	1.35	157.25	708.5	1.07	1.95	MC
45	166.75	692.3	0.01	2	169.08	567.6	0.02	1.86	169.75	534.1	0.21	1.96	169.88	535.8	0.08	1.98	
46	197.92	448.3	0.49	1.44	198.04	486	0.16	1.37	199.5	532	0.05	1.49	199.71	528.7	0.24	1.17	MC
47	227	425.2	0.39	1.45	227.13	424.1	0.18	1.5	227.88	396.5	0.07	1.61	228	378.7	0.46	1.05	
48	274.33	398.9	0.22	1.75	274.5	395.3	0.1	1.71	275.5	374.4	0.14	1.67	275.83	368.5	0.4	1.39	
49	275.96	372.3	0.48	1.25	276.04	392.4	1.14	1.19	277.13	393.2	0.08	1.48	277.29	398.5	0.81	1.52	
50	291.96	460.7	0.72	1.18	292.54	430.6	0.17	1.31	293.04	420.5	0.19	1.05	293.17	415	0.25	0.89	

Table I—Continued

No	t1 (DOY)	v1 (km s <sup>-1</sup> )	$\beta$ 1	Ar1	t2 (DOY)	v2 (km s <sup>-1</sup> )	$\beta$ 2	Ar2	t3 (DOY)	v3 (km s <sup>-1</sup> )	$\beta$ 3	Ar3	t4 (DOY)	v4 (km s <sup>-1</sup> )	$\beta$ 4	Ar4	Type
51	300.46	366	0.31	1.38	300.63	368.3	0.13	1.64	302.13	360.8	0.09	1.38	302.42	358.8	0.55	1.01	MC
52	308.17	501.8	0.76	1.4	308.92	514.8	0.12	1.87	309.58	497.9	0.02	1.34	309.83	492.1	0.96	1.39	
53	316.67	414.2	0.22	1.79	317.08	488.9	0.17	1.25	317.83	469.3	0.64	1.62	317.92	464.1	0.55	1.37	
54	325.63	385.8	1.63	1.59	325.75	388.3	0.31	1.76	327.71	371.1	0.18	1.47	327.79	369.6	0.28	1.55	
55	331.25	376.9	0.15	1.4	331.71	489	0.31	1.37	332.04	483	0.21	1.3	332.79	544.2	0.26	1.91	
56	346.63	434.5	0.5	1.23	346.83	440.6	0.17	1.51	348.46	403.2	0.19	1.84	348.88	409.4	0.1	1.62	MC